Three-Dimensional Characterization of Helical Silver Nanochains Mediated by Protein Assemblies

By *Frederic Leroux, Maarten Gysemans, Sara Bals,* Kees Joost Batenburg, Johan Snauwaert, Thierry Verbiest, Chris Van Haesendonck,** and *Gustaaf Van Tendeloo*

Biotemplate-based bottom-up fabrication can offer the high reproducibility and large-scale production that is generally lacked by top-down approaches when entering the nanometer regime. Nanometer-scale control of a high-quality, three-dimensional (3D) material structure is required for obtaining metamaterials with strong optical activity in the visible region. In particular, chiral metamaterials are of great interest because of the possibility to induce a negative index of refraction, resulting in unique optical functionalities that may be applied in novel types of optical devices such as superlenses.[1] Here, we demonstrate the use of insulin-derived fibrils as a biotemplate to grow helically arranged chains of silver nanoparticles with optical activity in the visible regime.

Despite the fact that biotemplating methods for nanodevice fabrication are becoming more widespread, characterization methods for their structural investigation remain widely unexplored. Whereas techniques such as atomic force microscopy (AFM) and transmission electron microscopy (TEM) are of crucial importance when studying conventional material structures, studies in which biotemplated nanostructures are characterized by TEM are limited because of specific problems that appear when investigating a combination of soft and hard matter by conventional TEM. The main difficulty is that the biomolecules are composed of very light atoms that do not contribute to the contrast in conventional bright-field TEM (BF-TEM) images. Soft-matter samples often require contrast enhancement by means of heavy-metal staining. However, heavy metals in the staining solution can induce artifacts and changes in the protein structure. Here, we show that an advanced TEM technique referred to as high-angle annular dark-field scanning transmission electron microscopy (HAADF-STEM) is very useful to study a combination of soft and hard matter. The 3D arrangement of the silver particles is crucial in order to understand the optical properties of these samples, and therefore discrete electron tomography was used to achieve a detailed structural characterization of the 3D self-organization and the true size of silver nanoparticles along the helix of the fibrils. This novel tomography technique was found to be essential when investigating samples that partially consist of beam-sensitive materials.

The use of biomolecules offers a large variety of new synthetic methods for the development of interesting nanostructured materials. These biotemplating methods take advantage of the characteristic nanometer dimensions of the biomolecules, together with the presence of well-defined functional groups at their surface. Recent studies used DNA strands[2] as a template to direct the deposition of inorganic components. Also microtubules have been metallized but are less suited because of their larger diameter around 25 nm.[3] Amyloid fibrils with a diameter close to 5 nm are other good candidates to serve as templates that remain stable under a variety of chemical conditions.[4] Amyloid fibrils are formed under conditions that destabilize the native state of proteins. They are best known for their association with neurodegenerative diseases such as Parkinson's disease and Alzheimer's disease and consequently their formation and structure have been studied extensively.[5] Scheibel et al.[6] and Padalkar et al.[7] have used amyloid protein fibrils as a scaffold to direct the deposition of inorganic materials in order to obtain conductive nanowires prepared in solution.

For our experiments bovine insulin was brought to polymerization under conditions of low pH and elevated temperature. This polymerization process resulted in insulin fibrils with diameters of 4 to 6 nm and lengths of several micrometers. The fibrils have a complex substructure, consisting of 2 to 6 intertwining protofilaments.[8] Next, the templates were metallized by electroless plating to obtain chains of nanoparticles. Insulin fibrils were incubated with silver ions in solution and subsequently immobilized on a substrate suitable for AFM or TEM measurements. After blotting off excess liquid, the silver ions were reduced by addition of a reducing agent. This results in the formation of metallic nanoparticles that are attached to active sites on the surface of the insulin template. During this procedure the support provided by the substrate stabilizes the fibrils.

In order to optimize the fabrication of nanostructured materials mediated by biotemplates, a thorough structural

[*] Dr. M. Gysemans, Prof. J. Snauwaert, Prof. C. Van Haesendonck
Laboratory of Solid-State Physics and Magnetism
Katholieke Universiteit Leuven
Celestijnenlaan 200 D, BE-3001 Leuven (Belgium)
E-mail: Chris.Van.Haesendonck@fys.kuleuven.be
F. Leroux, Prof. S. Bals, Prof. G. Van Tendeloo
EMAT, University of Antwerp
Groenenborgerlaan 171, BE-2020 Antwerp (Belgium)
E-mail: Sara.Bals@ua.ac.be
Dr. K. J. Batenburg
Vision Lab, University of Antwerp
Universiteitsplein 1, BE-2020 Wilrijk (Belgium)
Prof. T. Verbiest
Laboratory of Molecular Electronics and Photonics
Katholieke Universiteit Leuven
Celestijnenlaan 200 D, BE-3001 Leuven (Belgium)

DOI: 10.1002/adma.200903657

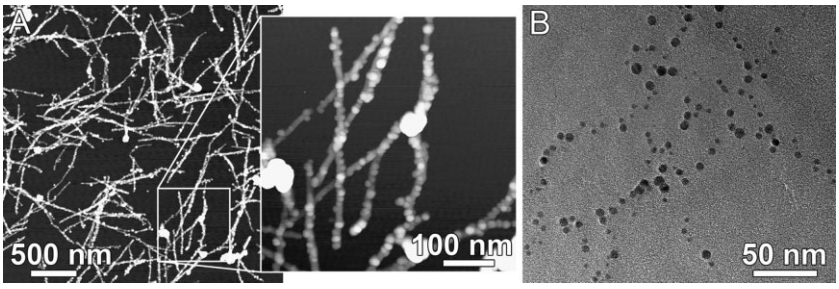

Figure 1. a) AFM image of insulin fibrils incubated with silver ions in solution, followed by deposition and reduction on the substrate. The fibrils reveal a dense covering with small silver particles. b) BF-TEM image in which only the silver particles are visible.

characterization is a prerequisite. AFM-based techniques have been used in the past to gain information on the morphology and the structure of metallized biomolecules.[9] Here, AFM measurements have been carried out on the metallized amyloid fibrils. The AFM image presented in Figure 1a shows fibrils with a granular appearance that are densely covered with spherical silver particles. Because of known tip-convolution effects in the lateral dimension, only the heights of the silver particles that lie directly on the substrate, sideways attached to the fibrils, were measured. The diameter of the particles was ranging from 3.5 to 6.5 nm and was in agreement with experiments that used a similar metallization method.[10]

Observation of metallized fibrils by BF-TEM reveals chains of silver particles, likely to be immobilized along amyloid templates (Fig. 1b). The morphology of the chains is consistent with the AFM observations. Next, we have measured the size of the fibril-bound particles from BF-TEM microscopy images. An average diameter of 4.6 nm ($\pm$1.2 nm) was found together with a distance between particles ranging from 2 to 5 nm.

High-resolution AFM images of metallized fibrils are presented in Figure 2a and 2b. The silver particles observed in the topography image (Fig. 2a) and phase image (Fig. 2b) have grown around the amyloid template. Both the fibril and the silver particles have diameters between 5 and 6 nm. Figure 2c presents a topography image of an unmetallized amyloid fibril with a diameter comparable to the fibril that is presented in Figure 2 and 2b. The bending patterns of the helical structure that is evident in Figure 2c can also be retrieved in the shape of the metallized fibril in Figure 2a and 2b.

In a next step, the nanochains were investigated using TEM. However, TEM studies in which combinations of biomolecules and inorganic materials have been investigated are usually based on conventional BF-TEM. The contrast in a BF-TEM image (see Fig. 1c) is dominated by the silver particles, since amyloid fibrils are difficult to resolve due to their light-atom composition. Based on the BF-TEM observations only, it is therefore impossible to draw reliable conclusions about the amyloid fibrils acting as a template for the deposition of the silver particles. In order to investigate the connectivity between the amyloid fibrils and the silver particles one has to use a technique in which both the biomolecules and the inorganic material yield sufficient contrast. Here, we propose an advanced TEM technique, HAADF-STEM, for this purpose. In HAADF-STEM mode, an HAADF detector will only collect electrons that have been scattered at high angles with respect to the optical axis, resulting in images where the intensity is approximately proportional to the square of the atomic number Z. Figure 2d shows an HAADF-STEM microscopy image of an insulin-derived amyloid fibril, confirming that HAADF-STEM allows us to directly image soft-matter samples. Based on the HAADF-STEM measurements, the diameter of the amyloid fibrils was found to range from 3 to 6 nm, which is in good agreement with the AFM results.

Additionally, HAADF-STEM was used to visualize silver-coated fibrils. Figure 2e shows a microscopy image in which contrast of both the biomolecules and the silver particles is present. This image should be compared to Figure 1b taken from another region in the same sample, where the contrast only originates from the silver particles. Obviously, HAADF-STEM proves to be an excellent technique to characterize hybrid inorganic–organic nanodevices. Based on Figure 2e, we can conclude that the particles are deposited along the amyloid fibrils, indicating that the silver patterns found earlier by BF-TEM are indeed mediated by the amyloid fibrils. In Figure 2f a coated fibril is shown in more detail. A helical pattern with a pitch of approximately 65 nm is clearly visible, consistent with the AFM measurements on fibrils that are not coated with silver particles. These observations suggest that the silver nanoparticles follow the 3D morphology of the amyloid fibrils that are known to have a helical structure.

The characterization methods introduced above have their limitations with respect to visualizing the morphology of the silver nanoparticles. TEM images have a good lateral resolution but provide only 2D projections of the 3D arrangement of the silver nanoparticles. AFM, on the other hand, has a good vertical

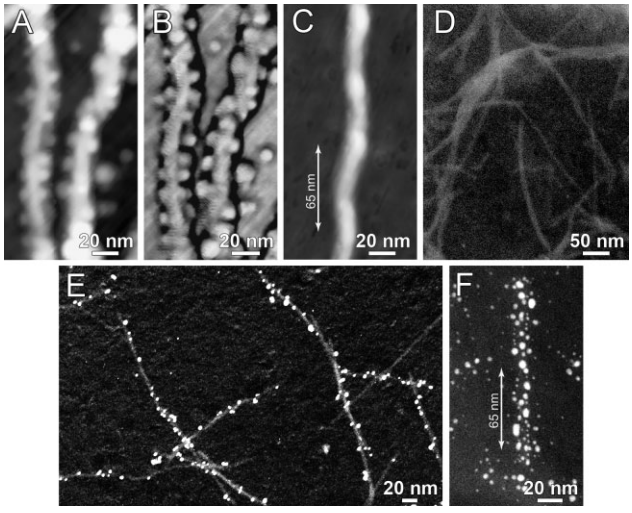

Figure 2. Topography a) and phase b) AFM images of fibrils with the silver particles that have grown around the fibrils. c) AFM topography image of an unmetallized fibril. d) HAADF-STEM image of uncoated fibrils. e) HAADF-STEM image of a silver-coated fibril (without staining). The silver particles are clearly distributed over the fibril surface. f) Detail of an unstained silver-coated amyloid fibril. The helix pitch was determined to be ~65 nm.

resolution but the lateral resolution is poor due to tip convolution effects. To overcome these limitations and to visualize the actual 3D arrangement and true size of the silver nanoparticles along the fibrils, a 3D reconstruction is required. This can be achieved by using electron tomography, where the 3D structure of an object can be obtained by collecting a large number of projection images at different tilt angles. After the acquisition, the projections serve as an input for a mathematical algorithm that allows the reconstruction of the 3D structure of the original object.

BF-TEM is a possible technique to obtain the projection images, but the change in diffraction contrast during tilting of crystalline samples causes artifacts in the reconstruction. To avoid these diffraction effects, HAADF-STEM was used again to acquire the images. Moreover, HAADF-STEM is better suited than conventional BF-TEM because of the higher signal-to-noise ratio and the reduced radiation damage. In our biotemplated nanochains, the nanoparticles are supported by beam-sensitive fibrils. Because of radiation damage on the biological part, the tilt range over which HAADF-STEM images have been acquired had to be limited to the range of angles between -68° and $+56^\circ$. This resulted in the so-called "missing wedge" of information that was rather large in this case and causes unavoidable elongation artifacts in the 3D reconstruction, which makes the reconstruction impossible to interpret. In order to overcome this problem, a recent technique known as "discrete tomography" was used. Discrete tomography is a new reconstruction technique, which has recently been applied to electron tomography for the first time.[11] It can be used to reconstruct 3D gray-scale volumes that contain only a small number of gray levels, typically corresponding to the different materials in the sample. Exploiting discreteness of the set of allowed gray levels in the reconstruction algorithm can reduce reconstruction artifacts, including missing-wedge-related artifacts. This makes discrete tomography a very attractive technique when studying samples partially consisting of beam-sensitive materials. Using discrete tomography, the 3D arrangement and morphology of the silver particles was investigated. During the reconstruction it was assumed that a pixel in the 2D projection images either represents silver or the carbon support, where both the fibrils and the carbon support are taken as a single gray level due to their low contrast difference. The result of this procedure is presented in Figure 3 (see also the Supporting Information for a 3D movie). A chiral arrangement of the particles is clearly visible, which proves that the nanoparticles indeed follow the helical morphology of the insulin fibril. To our knowledge, this is the first time that a biotemplated nanostructure is imaged with nanometer resolution using electron tomography.

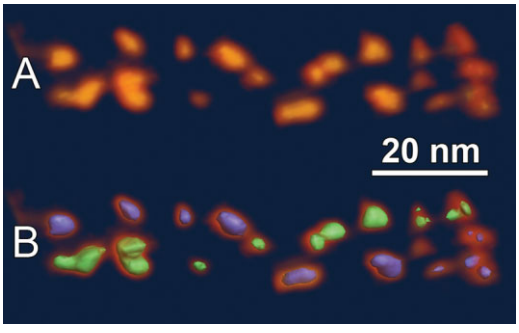

Figure 3. a) 3D reconstruction of a silver-coated fibril using a discrete algorithm. b) Colored overlay indicating the existence of a helical arrangement of the nanochain.

The organization of the silver particles on the helical insulin template was verified with circular dichroism spectroscopy. Circular dichroism spectroscopy is widely used to study biomolecules that exhibit circular dichroism in the far UV (around wavelengths of 200 nm) because of their secondary structure. Metal–protein interactions can be studied in the near-UV–visible (UV–vis) light region. Free metal particles in solution do not exhibit a circular dichroism signal and have to be incorporated in a chiral structure to produce such a signal. Figure 4 presents circular dichroism spectra of two samples: insulin fibrils at a concentration of 34 μM incubated with 5 mM silver ions (black) and insulin fibrils at a concentration of 0.14 mM incubated with 10 mM silver ions (gray). The curves presented in Figure 4 give the ellipticity (in millidegrees) as a function of the applied wavelength. We observe a circular dichroism band centered around 390 nm for the sample with lower insulin concentration and a broader band centered around 375 nm for the sample with the higher concentration. The presence of the circular dichroism band confirms that the silver particles, which are attached to the insulin fibrils, are organized according to a helix. The UV–vis absorbance spectrum of the sample incubated with a high concentration of metallized insulin fibrils is presented in the inset and reveals an absorbance peak centered around 410 nm. This is the wavelength region in which plasmon bands characteristic for metallic silver particles are typically observed in UV–vis spectroscopy. The absorption of UV light depends on the size and concentration of the silver particles, which can differ significantly from location to location on the sample. The position of the peak shifts to longer wavelengths with increasing size of the silver particles. The centers of the observed circular dichroism bands are located towards the lower wavelengths of the region in which we observe an UV–vis band.

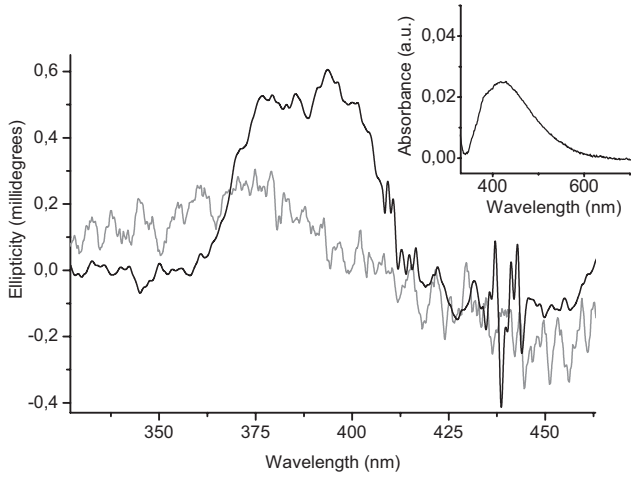

Figure 4. Circular dichroism spectra of insulin fibrils covered with silver and deposited on glass slides (black) at an insulin concentration of 0.034 mM, revealing a circular dichroism band centered around 390 nm and (gray) at an insulin concentration of 0.14 mM, revealing a wider circular dichroism band centered around 375 nm. The inset displays the UV–vis absorbance band of the sample with an insulin concentration of 0.14 mM.

This indicates that the smaller silver particles dominate the circular dichroism signal. This is consistent with our experimental observation (see Fig. 1) that the particles involved in the helical arrangement have a size of approximately 5 nm, while the larger silver aggregates are randomly distributed. The intensity of the observed circular dichroism signal is very low because we examined metallized fibrils deposited on a substrate. As a consequence, path length and amount of biomolecules that can be probed is very limited and the intensity of the observed CD bands becomes very low. Circular dichroism experiments are normally performed on liquid samples of optically active molecules in solution. This is impossible in our case as the metal particles are not attached to the biomolecules when applying the reduction step in solution.

The helical arrangement of the silver particles indicates that specific interactions occur between certain functional groups at the surface of the fibril and the silver ions. Future research will need to be directed towards a better understanding of these metal–protein interactions as this is a key requirement for the production and optimization of bioinorganic hybrid materials with specific physical and chemical properties.

In summary, we have demonstrated that electron tomography is a powerful technique to study the morphology and distribution of nanoparticles deposited along biomolecules. In order to obtain contrast from both the insulin fibrils as well as the inorganic material, without the use of heavy-metal staining, HAADF-STEM was used. HAADF-STEM was combined with the principle of electron tomography, but beam damage of the biomolecules hampered the collection of 2D projection images over a large tilt range. Therefore, we have shown that discrete tomography is a solution to this problem. Despite a rather large missing wedge, a good-quality 3D reconstruction was obtained where artifacts due to the missing wedge do not impede a straightforward interpretation. Here, the reconstruction allowed us to visualize the true morphology of the silver nanoparticles and to confirm that the particles follow the helical structure of the biomolecule used as a supporting scaffold in this study. This helical organization was further confirmed through circular dichroism spectroscopy. Therefore, the demonstrated method of HAADF-STEM discrete tomography provides a highly desirable advance towards the nanoscale 3D characterization of various nanodevices, especially in the domain of biotemplated nanomaterials. Finally, our experiments have revealed a possible way for the large-scale production of chiral metamaterials with tunable optical properties by relying on the attachment of metal particles at specific locations on a biomolecular template.

Experimental

Nanochain Synthesis: Bovine insulin (Sigma–Aldrich) was dissolved in water (3.5 mM), adjusted to pH 2 with HCl, and left to incubate at 70 °C for 2 h according to the protocol described by Jimenez et al. [4]. Next, metal particles are attached to active sites on the insulin fibrils by electroless plating. An aged $AgNO_3$ solution (5 mM) was added to the insulin fibrils (70 μM) and left to incubate overnight. Subsequently, the solution was deposited on a substrate and the excess liquid removed with a filter paper without completely drying the substrate, followed by reduction by putting a 20 μL drop of a $NaBH_4$ (5 mM) solution on the substrate. The samples were then rinsed with water and dried.

AFM: For the AFM measurements the fibrils were deposited on cleaned silicon oxide substrates. A Dimension 3000 system from Veeco Instruments was operated in tapping mode with PointProbe Plus cantilevers from Nanosensors with a force constant of 45 N m^{-1} and a resonance frequency of 270 kHz. High-resolution AFM measurements were performed with Hi'res-c tips from MikroMash with a force constant of 3.5 N m^{-1} and a resonance frequency of 75 kHz.

TEM: The samples for the TEM measurements were deposited on carbon-coated copper grids and silicon-monoxide-coated grids. Several TEM techniques were used to investigate the samples. The unstained metallized fibrils were analyzed by BF-TEM and high-resolution TEM (HRTEM), using a Philips CM30 operated at 300 kV. HAADF-STEM analysis of both Ag-coated and uncoated fibrils was carried out with a Jeol JEM-3000F TEM operated at 300 kV, to obtain contrast from unstained fibrils. Using the same microscope, HAADF-STEM images were also acquired over a tilt range of −68° to +56° for 3D reconstruction.

Optical Measurements: For the optical measurements, the insulin fibrils were deposited and metallized on cleaned optical-microscopy glass slides. The measurements were performed on a JASCO 62 DS setup.

Acknowledgements

F.L. and M.G. contributed equally to this work. S.B. and K.J.B are grateful to the Fund for Scientific Research Flanders (Contract nr. G.0247.08). We acknowledge financial support from the European Union under the Framework 6 program for an Integrated Infrastructure Initiative, Ref.: 026019 ESTEEM. Supporting Information is available online from Wiley InterScience or from the author.

Received: October 26, 2009
Published online: March 11, 2010

[1] a) J. B. Pendry, *Science* **2004**, *306*, 1353. b) S. Zhang, Y. S. Park, J. S. Li, X. C. Lu, W. L. Zhang, X. Zhang, *Phys. Rev. Lett.* **2009**, *102*, 1. c) E. Plum, J. Zhou, J. Dong, V. A. Fedotov, T. Koschny, C. M. Soukoulis, N. I. Zheludev, *Phys. Rev. B* **2009**, *79*, 1.

[2] a) C. Fang, Y. Fan, J. M. Kong, G. J. Zhang, L. Linn, S. Rafeah, *Sens. Actuators B* **2007**, *126*, 684. b) D. Haynie, G. Qun, C. Chuanding, S. Suryanarayanan, K. Dai, *Phys. E* **2006**, *33*, 92. c) S. E. Stanca, A. Ongaro, R. Eritja, D. Fitzmaurice, *Nanotechnology* **2005**, *16*, **1905**. d) Y. Zhousheng, C. Shiqiang, L. Yunchun, W. Xianwen, *Mater. Design* **2007**, *28*, 722. e) A. Zinchenko, K. Yoshikawa, D. Baigl, *Adv. Mater.* **2005**, *17*, 2820.

[3] S. Behrens, W. Habicht, J. Wu, E. Unger, *Surf. Interface Anal.* **2006**, *38*, 1014.

[4] a) S. L. Gras, *Aust. J. Chem.* **2007**, *60*, 333. b) T. P. J. Knowles, J. F. Smith, G. L. Devlin, C. M. Dobson, M. E. Welland, *Nanotechnology* **2007**, *18*, 1. c) J. L. Jimenez, E. J. Nettleton, M. Bouchard, C. V. Robinson, C. M. Dobson, H. R. Saibil, *Proc. Natl. Acad. Sci. USA* **2002**, *99*, 9196.

[5] a) J. F. Smith, T. P. J. Knowles, C. M. Dobson, C. E. MacPhee, M. E. Welland, *Proc. Natl. Acad. Sci. USA* **2006**, *103*, 15806. b) M. L. de la Paz, L. Serrano, *Proc. Natl. Acad. Sci. USA* **2004**, *101*, 87. c) W. S. Gosal, S. L. Myers, S. E. Radford, N. H. Thomson, *Protein Peptide Lett.* **2006**, *13*, 261. d) O. S. Makin, E. Atkins, P. Sikorski, J. Johansson, L. C. Serpell, *Proc. Natl. Acad. Sci. USA* **2005**, *102*, 315. e) J. Zurdo, J. I. Guijarro, C. M. Dobson, *J. Am. Chem. Soc.* **2001**, *123*, 8141.

[6] T. Scheibel, R. Parthasarathy, G. Sawicki, X. M. Lin, H. Jager, S. L. Lindquist, *Proc. Natl. Acad. Sci. USA* **2003**, *100*, 4527.

[7] S. Padalkar, J. D. Hulleman, S. M. Kim, J. C. Rochet, E. A. Stach, L. A. Stanciu, *Nanotechnology* **2008**, *19*, 1.

[8] R. Jansen, W. Dzwolak, R. Winter, *Biophys. J.* **2005**, *88*, 1344.

[9] a) R. M. Stoltenberg, A. T. Woolley, *Biomed. Microdevices* **2004**, *6*, 105. b) S. Pruneanu, S. A. F. Al-Said, L. Q. Dong, T. A. Hollis, M. A. Galindo, N. G. Wright, A. Houlton, B. R. Horrocks, *Adv. Funct. Mater.* **2008**, *18*, 2444. c) K. Keren, E. Braun, *Chem. Eng. Technol.* **2004**, *27*, 447.

d) R. Mohammadzadegan, H. Mohabatkar, M. H. Sheikhi, A. Safavi, M. B. Khajouee, *Phys. E* **2008**, *41*, 142. e) J. Zhou, G. Yao, A. Martinez-Molares, J. Xiaoye, Y. Dong, J. Lau, T. Hamasaki, C. Ozkan, M. Ozkan, E. Hu, B. Dunn, *Small* **2008**, *4*, 251.

[10] D. Liu, S. H. Park, J. H. Reif, T. H. Labean, *Proc. Natl. Acad. Sci. USA* **2004**, *101*, 717.

[11] a) S. Bals, K. J. Batenburg, J. Verbeeck, J. Sijbers, G. Van Tendeloo, *Nano Lett.* **2007**, *7*, 3669. b) K. J. Batenburg, S. Bals, J. Sijbers, C. Kubel, P. A. Midgley, J. C. Hernandez, U. Kaiser, E. R. Encina, E. A. Cornonado, G. Van Tendeloo, *Ultramicroscopy* **2009**, *109*, 730. c) S. Turner, S. M. F. Tavernier, G. Huyberechts, E. Biermans, S. Bals, K. J. Batenburg, G. Van Tendeloo, *J. Nanopart Res.* **2010**, *12*, 615.